

# Experimental and Numerical Investigation of Forced Convective Characteristics of Arrays of Channel Mounted Obstacles

T. J. Young

K. Vafai<sup>1</sup>

e-mail: vafai.1@osu.edu  
Fellow ASME

Department of Mechanical Engineering,  
The Ohio State University,  
206 W. 18th Avenue,  
Columbus, OH 43210

*An experimental investigation of the forced convective heat transfer of individual and arrays of multiple two-dimensional obstacles is reported. The airflow rate was varied from  $800 \leq Re_{D_h} \leq 13000$ . The effects upon the Nusselt numbers and obstacle temperature differences of parametric changes in the Reynolds number, channel height, array configuration, and input heat flux are established. The input heat fluxes to the obstacles ranged from  $950 \leq q'' \leq 20200 \text{ W/m}^2$ , which significantly extends beyond that seen in the open literature for forced convective air cooling of simulated electronic components. Comparisons of the obstacle mean Nusselt numbers are made with a two-dimensional laminar numerical model employing the Navier-Stokes equations. A set of correlations characterizing the heat transfer from the protruding heat sources within the channel is obtained. It was found that the obstacle temperature, the critical measure for electronic device failure, must be shown along with the corresponding Nusselt number to fully characterize the thermal state of the heated obstacle as the ratio definition of the Nusselt number can obscure large temperature increases. The results find that the proper placement of geometrically dissimilar obstacles, such as a taller obstacle, can be used to passively enhance the heat transfer in its vicinity. This effect would be dependent upon the flow rate and geometries in order to control the reattachment zones and their subsequent convective augmentation. The experimental results are found to be in good agreement with the results from the numerical simulation. Finally, a set of pertinent correlations for the arrays of channel mounted obstacles is given.*

## Introduction

The canonical model for the cooling of electronic devices, convective heat transfer from discrete heated obstacles in a channel, has been of interest for several decades (Peterson and Ortega, 1990). With each new generation of electronic devices that are further miniaturized and, concurrently, required to handle and dissipate larger energy loads, thermal management becomes the limiting operational factor (Mahefkey, 1995). In order to reduce localized hot spots, increase energy throughput, and reduce the failure rate, which is proportional to the exponential of the device junction temperature (U. S. DoD, 1991), thermal design of electronic components must necessarily be improved.

The forced convective cooling of flush-mounted and protruding two-dimensional heated obstacles in a channel was experimentally investigated by McEntire and Webb (1990). For an airflow range of  $10^3 \leq Re \leq 10^4$  and heat fluxes of  $850 \text{ W/m}^2$ , protruding heat sources were found to enhance the heat transfer compared with the flush sources. The characterization of turbulent flow and convective heat transport of single isolated two and three-dimensional obstacles in a channel was performed by Roeller et al. (1991). Larger obstacle widths increase the flow acceleration by blocking more channel flow area while

smaller widths have more intense three-dimensional transport effects.

The two-dimensional conjugate heat transfer problem for laminar flow over an array of three obstacles was solved, utilizing a control volume formulation, by Davalath and Bayazitoglu (1987). Their obstacles had uniform conductivity and were volumetrically heated. The spacing between the obstacles was varied from one to two times the obstacle width. Their analysis included the effects of obstacle spacing on the maximum temperature attained within the obstacles and the development of overall mean Nusselt number correlations of the form  $Nu_m = a Re^b Pr^c$  for the obstacles.

The use of an odd-sized rectangular obstacle within a three-dimensional array of square obstacles, with maximum heat fluxes of  $6700 \text{ W/m}^2$ , was found to enhance the heat transfer up to 40 percent by Jubran et al. (1996). Jubran and Al-Salaymeh (1996), using a similar experimental apparatus added spanwise ribs and spanwise "film cooling" to the obstacle array in order to enhance heat transfer up to 50 percent. Pressure drops were found to increase by nearly 70 percent when utilizing these techniques. Sparrow et al. (1984) also investigated the effects of height differences within three-dimensional arrays of square obstacles and found, using the naphthalene sublimation technique, heat transfer enhancements of up to 80 percent compared with an array of uniform height. A comprehensive experimental study of heat transfer in the entrance region of an array of rectangular heated blocks was presented in Molki et al. (1995).

In the previous studies, the periodicity within the ten obstacle array has been shown at the five percent difference level and at the less restrictive ten percent level. The mean Nusselt number,

<sup>1</sup> To whom correspondence should be addressed.

Contributed by the Heat Transfer Division for publication in the JOURNAL OF HEAT TRANSFER. Manuscript received by the Heat Transfer Division, Aug. 28, 1997; revision received, Apr. 15, 1998. Keywords: Convection, Cooling, Electronics, Enhancement, Experimental, Heat Transfer. Associate Technical Editor: M. Kaviany.

which reflects both fluid and thermal conditions, for eight and seventh obstacles were within five percent and ten percent, respectively, of the value found at the ninth obstacle. The local values of the velocity components and temperature at the “periodic” boundaries clarify and support the use of periodic boundary conditions for obstacles that are assumed to be located away from the entrance. Comparisons with experimental work shows similar results. Lehmann and Pembroke (1991) reported  $Nu_m$  being constant, within experimental uncertainty, for rows six to ten. Garimella and Eibeck (1990) reported that the heat transfer coefficient was asymptotic by the fourth row in their experiments.

This work presents a systematic and thorough investigation of forced convective cooling of a two-dimensional array of multiple heated obstacles located upon one wall of an insulated channel. Experiments were performed for a generic set of obstacles representative of an electronics cooling configuration over a range of geometries, input thermal energies, and airflow rates. The experiments were carried out over a range of Reynolds numbers,  $800 \leq Re_{D_h} \leq 13000$ , typical of forced air cooled electronics. The input heat flux to the test articles mounted within the channel ranged from  $950 \leq q'' \leq 20200 \text{ W/m}^2$ . This input heat flux range significantly extends that seen in the open literature for forced air cooling experiments of heated obstacles. The influences of parametric changes in the obstacle geometry, spacing, number, thermal conductivity, and heating method, at various flow rates, upon the flow and heat transfer were examined prior to experimentation to isolate the important criteria for performing the tests. The dependence of the streamlines, isotherms, and Nusselt numbers on the governing parameters was studied. The different geometric arrangements that were employed to study the effects upon the heat transfer include changes in the channel height and the use of an individual obstacle or an array of five similar obstacles. The effect of the position of a taller obstacle within an array was also investigated. It is shown that very large heat fluxes approach the limits for sensible heat convective transport while substantially increasing the obstacle to coolant temperature difference. The use of a taller obstacle in an array was found to provide heat transfer enhancement downstream as the core flow expands, providing a method to tune thermal transport at specific positions.

## Experimental Apparatus and Procedure

The test channel which was constructed to study the forced convective heat transfer of the heated test articles, including the entrance and outlet plenums and the related test and measurement equipment, is shown in Fig. 1. The setup was designed for accurate measurements as well as enabling a wide range of adjustments in the relevant parameters, such as Reynolds number, channel height, and obstacle number and spacing. The purpose of the experiments is to obtain the temperatures and con-

vective heat transfer coefficients at the obstacle surfaces for various coolant rates and obstacle arrangements.

As shown in Fig. 2, the channel walls, floor, and base were constructed of 12.7-mm-thick clear acrylic ( $k \approx 0.2 \text{ W/m} \cdot \text{K}$ ) while the ceiling was 6.4-mm-thick clear acrylic. The test channel has a length of 2.5 m with approximately 1.7 m between the entrance and test section. Slots in the vertical walls permit ceiling assembly adjustments to be made that allow a channel height range of about  $H = 10$  to 90 mm. The channel width was fixed at  $W = 305 \text{ mm}$  to reduce end effects upon the measurements made along the channel spanwise centerline. Roeller et al. (1991) found, for a similar channel arrangement, that the end wall effects were limited to ten percent of the channel width. All joints were sealed with silicone rubber sealant or vinyl tape to ensure that no air leakage occurred. At the channel entrance, isolation from the ambient environment is achieved using a large cubical plenum (0.8 m each side) with multiple screens positioned at the inlet. A honeycomb structure assures smooth airflow transition into the test channel. At the channel outlet, a 0.4-m-long plenum with a gradual rectangular to circular transition employs several layers of fine mesh to isolate the test channel from downstream influences.

A regenerative blower, rated at 4 to 80 SCFM and operating in suction mode to reduce airflow disturbances within the test channel, drew air through the test channel and to the appropriate orifice plate bypass flow meter (AquaMatic FLT series) depending upon the desired flow rate. The factor calibration of the flow meters showed accuracy of better than two percent. The recommended lengths of straight pipe were installed before and after the orifice plates to ensure accurate measurements. The exhaust air was routed away from the experimental apparatus to avoid tainting the inlet air or measurement of ambient conditions.

The test articles that were mounted within the flow channel were machined from solid 6061-T6 aluminum alloy ( $k = 165 \text{ W/m} \cdot \text{K}$ ). As shown in the details of Fig. 2, a 3.2-mm-deep cavity for the heater was machined into the obstacle base in order to provide an insulative air gap between the obstacle and the channel floor. The contact areas between the obstacle base and the channel floor are only 1.6 mm wide across nearly the entire channel width in order to reduce conductive losses to the channel floor. The exposed obstacle surfaces were polished with very fine steel wool prior to testing. The obstacles were firmly affixed to horizontal slots in the test section vertical walls. This arrangement allowed the obstacle number and spacing within the test section to be varied. Two different obstacle sizes were employed in this work: 28.6\_25.4\_305 mm and 28.6\_12.7\_305 mm (streamwise length, height, and spanwise width, respectively).

The constant heat flux at the base of the test articles was applied using thin-film etched foil heaters (Watlow Electric)

## Nomenclature

**A, B, C, D** = obstacle corners  
 $D_h$  = channel hydraulic diameter, m  
 $h$  = obstacle height, m  
 $h_c$  = convective heat transfer coefficient,  $\text{W}/(\text{m}^2 \cdot \text{K})$   
 $H$  = channel height, m  
 $k$  = thermal conductivity,  $\text{W}/(\text{m} \cdot \text{K})$   
 $L$  = obstacle streamwise length, m  
 $Nu$  = Nusselt number,  $h_c H / k_f$   
 $Pe_H$  = Péclet number,  $\rho_f c_p u_m H / k_f$

$q$  = heat transfer rate, W  
 $q''$  = heat flux,  $\text{W}/\text{m}^2$   
 $Re_{D_h}$  = Reynolds number,  $\rho_f u_m D_h / \mu_f$   
 $s$  = obstacle spacing, m  
 $T$  = temperature,  $^\circ\text{C}$   
 $u$  = velocity, m/s  
 $W$  = channel width, m  
 $\mu$  = dynamic viscosity,  $(\text{N} \cdot \text{s})/\text{m}^2$   
 $\rho$  = density,  $\text{kg}/\text{m}^3$   
 $\Theta$  = dimensionless temperature,  $(T - T_e)/(q'' H / k_f)$

## Subscripts

$e$  = entrance  
 $elec$  = electrical  
 $f$  = fluid  
 $m$  = mean  
 $s$  = solid  
 $w$  = wall

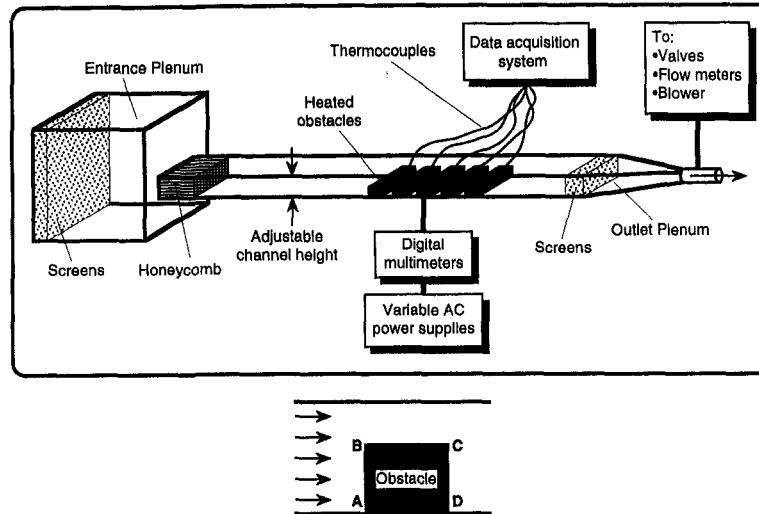


Fig. 1 Schematic diagrams of the experimental apparatus and heated obstacle edge view

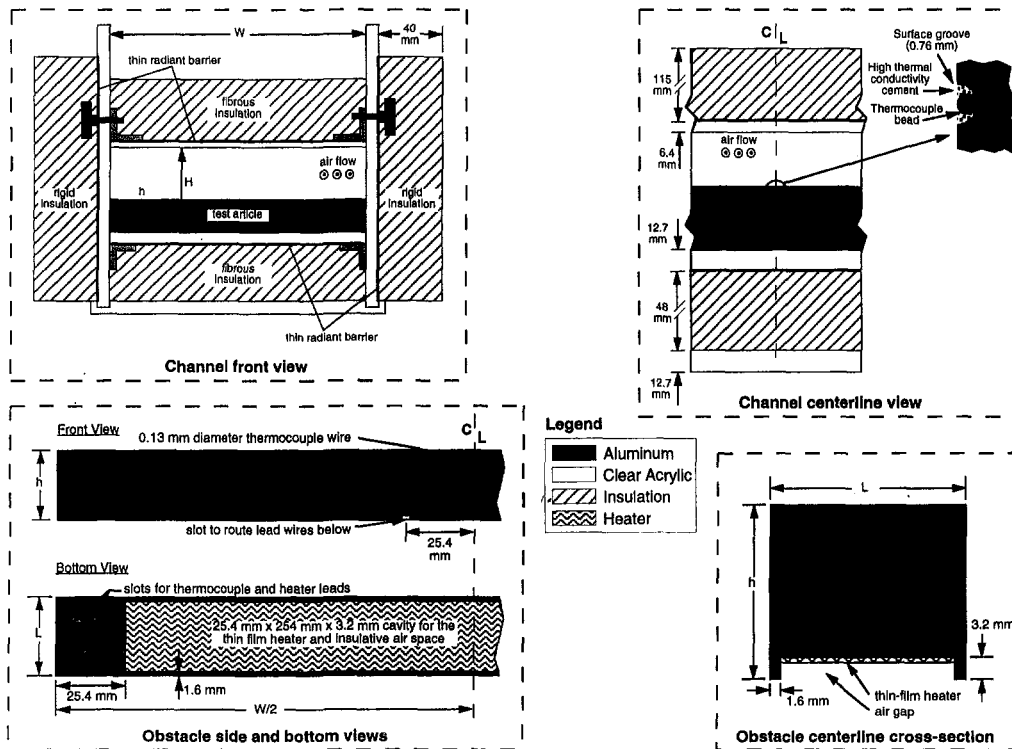


Fig. 2 Details of the experimental test channel and test articles

rated at 100 watts with length 254 mm and width 25.4 mm. An unheated spanwise length of 25.4 mm was situated adjacent to the obstacle attachment points. The heaters were attached to the obstacles by means of a pressure-sensitive adhesive capable of providing good thermal contact. To reduce radiative losses, the downward-facing exposed heater surface was coated with a reflective low-loss coating while a thin reflective barrier was applied immediately outside the four channel walls. Conductive losses from the channel were reduced through the use of fibrous insulation ( $k \approx 0.04 \text{ W/m}\cdot\text{K}$ ) at the channel top (115 mm thick) and bottom (48-mm-thick) surfaces and expanded polystyrene insulation ( $k \approx 0.07 \text{ W/m}\cdot\text{K}$ ), 40 mm thick, along the vertical channel surfaces.

In order to accurately measure the temperature of the wetted surfaces, the aluminum obstacles were instrumented by embedding thin (36 AWG) Type-E thermocouples in very small (0.76 mm) surface grooves designed to minimize flow disturbances (Fig. 2). The thermocouple beads were located along the spanwise obstacle centerline ( $W/2$ ). The lead wires were led away from the centerline in the grooves and routed underneath the obstacle to avoid disturbing the airflow. High thermal conductivity cement (Omega OB-400) was used to hold the thermocouples in place and completely fill the grooves in order to minimize the effects of removing material from the obstacles. The taller obstacles employed ten thermocouples: four on the top surface (BC) and three each on the up (AB) and down-

stream (CD) surfaces. The shorter obstacles had eight thermocouples: four on the top surface (BC) and two each on the vertical (AB and CD) surfaces. One thermocouple was employed outside the test channel to measure the ambient air temperature.

The electrical power to each heater under test was supplied by a separate a-c autotransformer. The variable output of the autotransformers allowed precise and individual control of up to 140 VAC (at  $\pm 0.5$  percent or better) to be furnished to the heaters. The RMS voltages and currents were measured using calibrated digital multimeters. The thermocouple signals were amplified, filtered, and multiplexed near the test section to reduce noise corruption and signal errors.

The experimental site was a very large volume room capable of absorbing the warm airflow output from the blower without affecting the ambient conditions. The experiments were performed meticulously, for example, through verifications of adjusted dimensions with digital calipers, thorough cleanings of the test channel interior, and regular observations of the flow rate and the heater input powers. To begin the experiments the blower was first metered to the desired flow rate. The required input power to the heaters was then supplied by the autotransformers while the voltage and current were recorded for heat flux calculations. The obstacle temperatures were continuously monitored until steady-state conditions were reached (approximately 45 to 300 minutes, depending upon airflow rate and heater power). A data acquisition system was used to gather and process the thermocouple signals and perform data reduction. To verify the attainment of steady conditions, several experiments were run after the steady-state conditions were attained to supply additional data for comparison. Duplicate experimental runs were performed at each test, and on different days, to verify the repeatability of the results.

**Data Reduction.** The local convective heat transfer coefficient on the obstacle surface was defined as

$$h_c = \frac{q}{A_c(T - T_e)} \quad (1)$$

where the convective heat transfer,  $q$ , was calculated from

$$q = q_{\text{elec}} - (q_{\text{cond}} + q_{\text{rad}} + q_{\text{lw}}). \quad (2)$$

In the above expressions  $A_c$  is the test article wetted surface area,  $T$  and  $T_e$  are the local surface and ambient temperatures, respectively,  $q_{\text{elec}} = EI$  is the total electrical power input to the heater, and  $q_{\text{cond}}$ ,  $q_{\text{rad}}$ , and  $q_{\text{lw}}$  are the heat losses due to conduction, radiation, and lead wire conduction, respectively. The conduction heat loss was estimated at four percent using measurements of the temperature drop across the channel walls and through use of a miniature heat flux sensor (Concept Engineering) located beneath the channel floor. The radiation loss was estimated at two percent while a one-dimensional conduction analysis found the heater lead wire loss to be less than one percent and was combined into the conduction loss estimate. Each temperature value ( $T$ ,  $T_e$ ) gathered was the mean of 100 readings. The standard deviation for these sets of temperatures was found to vary between 0.005 and 0.15°C.

The local Nusselt number was defined as  $Nu = h_c H / k_f$ . The mean Nusselt number was found as the average of the local values,

$$Nu_m = \frac{\int_{A_c} Nu \, dx}{A_c}. \quad (3)$$

The Reynolds number was defined as  $Re_{D_h} = \rho_f u_m D_h / \mu_f$ , where the mean fluid velocity,  $u_m$ , was found from the volumetric flow rate within the channel and the channel hydraulic diam-

eter is  $D_h = 2WH / (W + H)$ . All thermophysical properties of the air were evaluated at the entrance temperature.

**Experimental Uncertainty.** An error analysis utilizing the method of Kline and McClintock (1953), as extended by Moffat (1988), was performed to evaluate the uncertainty in the experimental data. The relative uncertainty of dependent variable  $R = f(\lambda_i)$  was obtained using

$$\frac{\delta R}{R} = \left[ \sum_{i=1}^N \left( \frac{\delta \lambda_i}{\lambda_i} \right)^2 \right]^{1/2}. \quad (4)$$

Best and worst-case values were assessed for the uncertainties in the relevant independent variables. The  $N$ th-order uncertainty in the Nusselt numbers obtained was calculated to lie between 4.3 and 8.5 percent whereas that in the Reynolds numbers was between 3.5 and 7.7 percent. A first-order uncertainty estimate of the data scatter (Moffat, 1988) found that, in 25 repeated trials, the standard deviation of the measured temperature difference  $T - T_e$  for the ten thermocouples on an individual obstacle was less than one percent.

## Numerical Analysis and Procedure

A numerical model for the convective cooling of heated obstacle arrays located in a two-dimensional insulated wall channel was developed and utilized for comparative purposes. The Navier-Stokes equations for the laminar flow of a steady incompressible Newtonian fluid with constant thermophysical properties were solved, fully accounting for the conductive energy flow through the solid obstacles. The governing conservation equations are

### Mass

$$\frac{\partial u_i}{\partial x_i} = 0. \quad (5)$$

### Momentum

$$Re_H \left( u_k \frac{\partial u_j}{\partial x_k} \right) = - \frac{\partial p}{\partial x_j} + \frac{\partial^2 u_j}{\partial x_i \partial x_i}. \quad (6)$$

### Energy (fluid)

$$Pe_H \left( u_j \frac{\partial \Theta_f}{\partial x_j} \right) = \frac{\partial^2 \Theta_f}{\partial x_i \partial x_i}. \quad (7)$$

### Energy (solid)

$$\frac{\partial^2 \Theta_s}{\partial x_i \partial x_i} = 0. \quad (8)$$

Boundary conditions were specified along the entire solution domain due to the elliptic nature of the governing equations. At the obstacle bases, a constant surface heat flux was applied.

### Entrance

$$u = 6y(1 - y), \quad v = 0, \quad \Theta_f = 0. \quad (9)$$

### Outlet

$$\frac{\partial u}{\partial x} = 0, \quad \frac{\partial v}{\partial x} = 0, \quad \frac{\partial \Theta_f}{\partial x} = 0. \quad (10)$$

### Fluid/solid interfaces

$$u = 0, \quad v = 0, \quad \Theta_f = \Theta_s, \quad k_f \frac{\partial \Theta_f}{\partial \mathbf{n}} = k_s \frac{\partial \Theta_s}{\partial \mathbf{n}}. \quad (11)$$

### Channel walls

$$u = 0, \quad v = 0, \quad \frac{\partial \Theta_f}{\partial y} = 0. \quad (12)$$

The system of equations that are being solved as well as the boundary conditions are of the elliptic form. The reason that the boundary conditions at the right-hand side of the domain are not explicitly specified is explained in what follows (this is already partly discussed in the text but in the revised manuscript this discussion has been expanded). The fact that needs to be mentioned in here is, through extensive numerical experimentation, it was discovered that the boundary conditions on the right-hand side of the computational domain have a limited effect on the upstream results. In fact, this influence was usually not more than ten grid points upstream due to the strong parabolic nature of the problem. Hence, the type of boundary condition specification on the right-hand side of the computational domain did not have much influence on the physical domain. Therefore, by using an extended computational domain, very accurate results for our physical domain were performed. That is, the computational domain was always chosen to be larger than the physical domain. Extensive tests on the effect of varying the size of the computational domain were run, and its effects on the physical domain were observed to ensure that the boundary conditions on the downstream side of the computational domain (the right-hand side) had no influence on the results. In our work, for simplicity, the conditions at the last interior grid points from the outflow boundary condition in the previous iteration were used and it yielded the same solution for the domain of interest except for the region very close (this is the region which was part of our computational domain but not the physical domain) to the downstream boundary as when the other conditions were used.

Indeed, this mesh was designed to capture the critical features near the obstacle region and to provide sufficient mesh density, with minimal element distortion, at the obstacle surfaces. Extensive tests, involving mesh densities and gradings, were performed to confirm the grid independence of the model until further refinement showed less than a one-percent difference in the results. To eliminate the influences of the entrance and outlet upon the solution near the obstacle region, as described by Vafai and Kim (1990), additional tests were performed by individually increasing the lengths of the channel before and after the obstacle array. Entrance effects were found to be effectively isolated with  $L_e = 2$ . An outlet length of  $L_o = 8$  ensured that the large downstream recirculation zone was well ahead of the outlet and that the fluid exited in a parabolic profile. Therefore, the problem was solved without making any assumptions regarding a periodic boundary condition and as such the solution is more accurate.

The local Nusselt numbers, found from  $Nu = h_c H / k_f = -\Theta_w^{-1} (\partial \Theta_f / \partial \mathbf{n})$ , where  $\mathbf{n}$  is the surface normal, were averaged to obtain the mean obstacle Nusselt numbers. Because of the geometric differences between the experimental flow channel and the two-dimensional model, a geometric factor was utilized to allow comparison between the Reynolds numbers. The mean fluid velocities ( $u_m$ ) in the Reynolds number definitions for the numerical and experimental methods were equalized, which resulted in the ratio  $Re_{exp}/Re_{num} = W/(W + H)$ , allowing the numerical results to be compared with the experimental data.

To validate the numerical scheme used in the present investigation, comparisons with previous studies were performed. This was achieved through adjustments to the model to match the geometric, hydrodynamic, and thermal conditions of the related works. First, comparisons were made with the analytical solutions of Cess and Shaffer (1959a, b) with respect to the problems of thermal entry length in a channel with constant wall temperature or heat flux. Calculated entrance region and fully developed Nusselt numbers showed excellent agreement. Next, a hydrodynamic comparison with the single obstacle case of Zebib and Wo (1989) was made. Thermal comparisons were not made due to lack of information for their multiconductivity obstacle and the multilayer channel walls with a constant con-

vective coefficient beneath the bottom surface. Their three inlet velocities correspond to  $Re_{D_h} = 806, 1772, \text{ and } 3222$ . A comparison of the recirculation zone and reattachment length behind the obstacle was within  $\sim 2$  percent for the lowest two Reynolds numbers and within  $\sim 8$  percent for the highest (run as laminar flow even though the Reynolds number was well within the transition regime).

The solution to the governing equations was found through the Galerkin finite element method (FIDAP, 1993). A highly variable mesh was employed to capture the critical features near the obstacle regions and to provide sufficient mesh density, with minimal element distortion, at the obstacle surfaces. Extensive tests, involving mesh densities and gradings, were performed to confirm the grid independence of the model. Complete details of the solution scheme and the extensive validation studies can be found in Young and Vafai (1998a, b) and will not be presented for brevity.

## Results

The experiments reported here fall into three distinct classes based upon the number and geometry of the test articles located within the channel: an individual obstacle, an array of five, similar obstacles, and an array of four obstacles incorporating one taller obstacle. The study included the effects of changes in the Reynolds number,  $Re_{D_h}$ , input electrical power to the heaters,  $q_{elec}$ , and channel height,  $H$ , upon the heat transfer, characterized by the Nusselt number. The Reynolds number ranged from  $800 \leq Re_{D_h} \leq 13000$  while the input electrical power imposed upon the heaters,  $q_{elec} = EI$ , ranged from 6.1 to 130.2 W ( $950 \leq q_{elec}'' \leq 20200 \text{ W/m}^2$ , where  $q_{elec}'' = q_{elec}/A_h$  and  $A_h$  is the heater-obstacle contact area). Measured temperature differences ranged from  $3 \leq T_m - T_c \leq 148^\circ\text{C}$ . The streamwise length of the obstacles,  $L$ , was chosen to nondimensionalize the geometric data as it remained constant at  $L = 28.6$  mm. Two obstacle heights were thus employed,  $h/L = 0.44$  and 0.89, while the channel height varied in the range of  $1.22 \leq H/L \leq 3.11$ .

**Single Obstacle.** For these experiments a single obstacle was placed within the test channel. Numerical results corresponding to some experimental runs were obtained using the method described above. Presented in Fig. 3(a) are comparisons between the experimentally and numerically obtained mean Nusselt numbers for an individual heated obstacle of height  $h/L = 0.89$  in a channel of height  $H/L = 3.11$ . The numerical model is seen to slightly over predict the Nusselt number as the Reynolds number increases, from 3.6 percent at  $Re = 770$  to 13.6 percent at  $Re = 1530$ . Overall, the agreement is very good and it was observed that the experimental and numerical results display the same trends in the Nusselt number with changes in the airflow rate. Similar comparative results between the experimental and numerical data are shown in Fig. 3(b) for an individual obstacle of height  $h/L = 0.44$  within the channel of height  $H/L = 3.11$  in the laminar regime.

To provide a baseline for the parametric analyses and for further comparison, a single obstacle of height  $h/L = 0.89$  was placed within the test channel of height  $H/L = 1.57$ . The mean Nusselt numbers of the single obstacle, for  $800 \leq Re_{D_h} \leq 13000$ , and an input power of  $q_{elec} = 54.6 \text{ W}$  ( $q_{elec}'' = 8500 \text{ W/m}^2$ ), were found and compared with the composite correlation of Roeller et al. (1991) developed for a range of obstacle geometries. Figure 4 shows the experimental mean Nusselt number data for the parameters given above and two correlations. The first is the least-squares correlation developed for the experimental data,

$$Nu_m = 0.4472 Re_{D_h}^{0.5618}, \quad (13)$$

with  $R^2 = 0.96$ , for the wide range of Reynolds numbers, 800

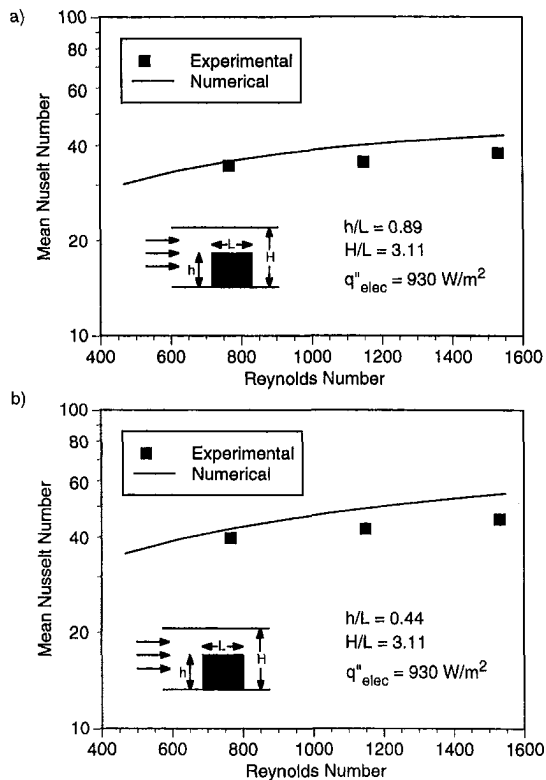


Fig. 3 Mean Nusselt number comparison between the experimental and numerical analyses for  $h/L = 0.89$ ,  $H/L = 3.11$ , and  $q''_{elec} = 930 \text{ W/m}^2$

$\leq Re_{D_h} \leq 13000$ . The second curve is the composite correlation recommended by Roeller et al. (1991),  $Nu_m = 0.454 Re_{D_h}^{0.555}$ , for the given geometries. The experimental data of Fig. 3 is matched fairly well by either correlation, with the correlation of Roeller et al. (1991), thereby corroborating the current results.

The mean Nusselt number at  $Re_{D_h} = 13000$  in Fig. 4, considered as the baseline single-obstacle case ( $Nu_{m0} = 105.7$ ), was used to normalize the mean Nusselt numbers presented in the parametric results of Fig. 5. An increase in mean Nusselt number with increased Reynolds number, for fixed geometry and input electrical power, is shown in Fig. 5(a). As the flow rate, and consequently the convective heat transfer was increased, the average surface temperature difference decreased from about  $147^\circ\text{C}$  to  $32^\circ\text{C}$ . With this large imposed heat flux, large

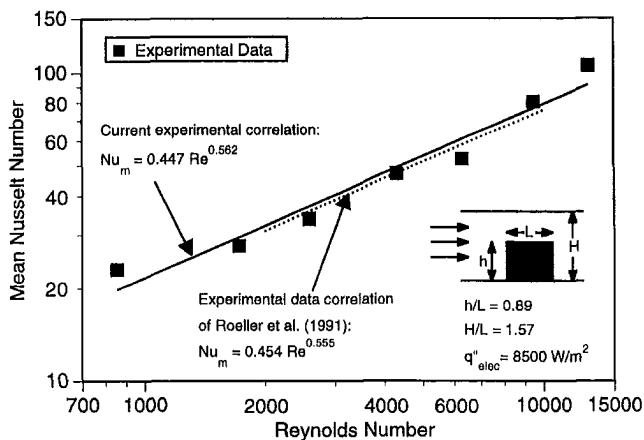


Fig. 4 Comparison of the experimental data for  $h/L = 0.89$ ,  $H/L = 1.57$ , and  $q''_{elec} = 8500 \text{ W/m}^2$  with the correlation developed by Roeller et al. (1991)

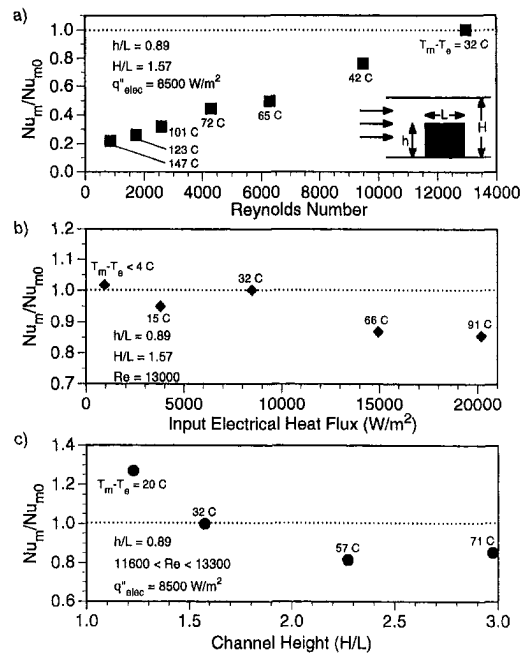


Fig. 5 Mean Nusselt number comparisons, and corresponding temperature differences, between the single obstacle baseline case ( $Nu_{m0} = 105.7$ ) and cases with parametric variations in (a) Reynolds number, (b) input electrical power to the heater, and (c) channel height

airflow rates are required to keep the obstacle temperatures, and corresponding electronic device failure rates, low. Figure 5(b) reports the results found when at a fixed geometry ( $h/L = 0.89$ ,  $H/L = 1.57$ ) and airflow rate ( $Re_{D_h} = 13000$ ), the electrical power input to the heater is parametrically varied from 6 W to 130 W ( $950 \leq q''_{elec} \leq 20200 \text{ W/m}^2$ ). The Nusselt numbers are roughly grouped into two regions. At the lower heat fluxes the Nusselt numbers are within  $\pm 5$  percent of that of the baseline. At the larger heat fluxes the trend is for the Nusselt numbers to decrease with increasing heat flux. Though the decrease in Nusselt numbers is small as the input heat flux increases from about 15 to 20  $\text{kW/m}^2$ , the temperature difference increases considerably. Such temperature increases have the potential to destroy electronic devices, though this is not immediately apparent when consulting the dimensionless parameters because the  $q/(T - T_e)$  ratio in the Nusselt number definition (Eq. (1)) decreases slightly as the heater input power is increased. The general decrease in mean Nusselt numbers at greater heater input powers suggests that the forced convective heat transfer limit for direct air cooling is being approached (Peterson and Ortega, 1990).

The effect that a change in channel height ( $1.22 \leq H/L \leq 2.97$ ) for fixed-obstacle size, airflow rate, and input heater power has upon the mean heat transfer is shown in Fig. 5(c). The Reynolds number, for fixed airflow rate, changes about 15 percent due to the channel height variation. When the channel height is at its lowest value, the airflow velocity through the bypass region increases, causing an increase in the convective heat transfer and a corresponding reduction in obstacle temperature compared with the baseline case. The Nusselt number for the largest channel height ( $H/L = 2.97$ ) was found to be about five percent greater than for  $H/L = 2.27$ , though the larger channel height case has a surface temperature difference of about  $14^\circ\text{C}$  greater than that for  $H/L = 2.27$ . Again, due to the exponential dependence of electronic device failure on temperature (U. S. DoD, 1991), hidden temperature increases, such as these, need to be accounted for. A local minimum in the Nusselt number versus channel height curve is expected as this curve should have positive concavity. Consider the mean Nusselt number definition  $Nu_m = (h_c)_m H / k_f \propto H / (T_m - T_e)$ . At the

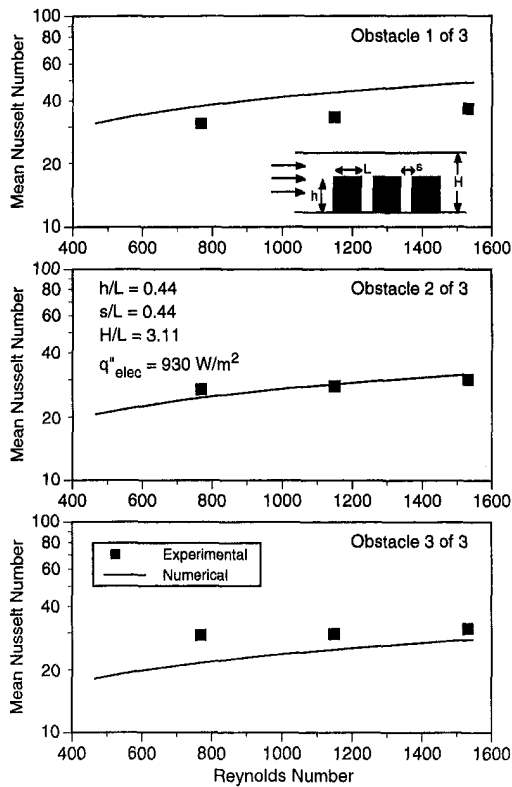


Fig. 6 Mean Nusselt number comparisons between the experimental and numerical results for a three obstacle array with  $h/L = 0.44$ ,  $s/L = 0.44$ ,  $H/L = 3.11$ , and  $q''_{elec} = 930 \text{ W/m}^2$

smallest channel heights ( $H$ ), with the resulting greater mean channel airflow velocities ( $u_m$ ), the reduced obstacle temperature difference dominates the Nusselt number. As the channel height increases, the mean airflow velocity decreases, reducing the convective transport at the obstacle and increasing its temperature. Near the local minimum neither  $H$  nor  $(T_m - T_e)$  dominates the Nusselt number. However, as the channel height increases beyond the local minimum, its increases are greater than the resulting increases in temperature difference, causing the ratio  $H/(T_m - T_e)$ , and, hence, the Nusselt number, to increase. Consider dramatic increases in channel height (beyond the heights given in the current experimental apparatus) where the changes in temperature would be small compared with the increases in  $H$ , resulting in an “artificial” increase in Nusselt number.

**Multiple Obstacle Arrays.** The numerical analysis was utilized to compare the mean convective heat transfer behavior for the system-like configuration of an array of three heated obstacles of height  $h/L = 0.44$  and inter-obstacle spacing  $s/L = 0.44$  within a channel of height  $H/L = 3.11$ . For the experiments the input heat flux was  $q''_{elec} = 930 \text{ W/m}^2$  while the airflow was kept within the laminar regime. Figure 6 shows, for the three obstacles, the mean Nusselt number comparison between the experimental and numerical analyses. Both analyses show the trends of increased Nusselt number with increases in Reynolds number and decreased convective heat transfer with downstream obstacle position. For each of these trends, the numerical analysis, however, shows differences, such as a greater Nusselt number increase with increased flow rate and larger Nusselt number decreases with downstream position. A similar comparison for an array of five obstacles with the geometry  $h/L = 0.89$ ,  $s/L = 1.0$ , and  $H/L = 3.11$ , is shown in Fig. 7. A reduction in the disparities between the experimental and numerical results could come with an increase in the sophisticated

tion of the numerical model to include three dimensions and low Reynolds number turbulence modeling, for example.

For the set of multiple obstacle array experiments, two different test article geometries were considered. In the first case, five identical obstacles of height  $h/L = 0.89$  and inter-obstacle spacing  $s/L = 1.0$  were placed within the channel of height  $H/L = 1.57$ . In the second case, four obstacles of identical streamwise length and spacing ( $s/L = 0.72$ ) were utilized, but three obstacles were of height  $h_2/L = 0.44$  while one was  $h/L = 0.89$ . The taller obstacle was systematically positioned in all four possible locations within this array configuration to investigate its effect upon the convective heat transfer.

The experimental mean Nusselt numbers for the five obstacle array at  $2500 \leq Re_{D_h} \leq 13000$  and  $q''_{elec} = 3750 \text{ W/m}^2$  are shown in Fig. 8. An effort was made to compare this Nusselt number data for the five heated obstacles with other experimental works. McEntire and Webb (1990) tested an array of four two-dimensional surface-heated-only thermally insulative obstacles. Their composite relation for the mean convective heat transport considering all four obstacles in their array, over the range  $1850 \leq Re_{D_h} \leq 9300$ , was  $Nu_m \propto Re^{0.61}$ . As shown in Fig. 8, this composite correlation over predicts the data generated in the current experimental apparatus, which is to be expected as the insulative obstacles employed by McEntire and Webb (1990) eliminate the reduced convective transport from the vertical obstacle surfaces. The mean Nusselt numbers shown in Fig. 8 do account for the reduced convective behavior along the vertical surfaces of the conducting obstacles and, as a result, show lower Nusselt numbers than the composite correlation of McEntire and Webb (1990). However, the least-squares corre-

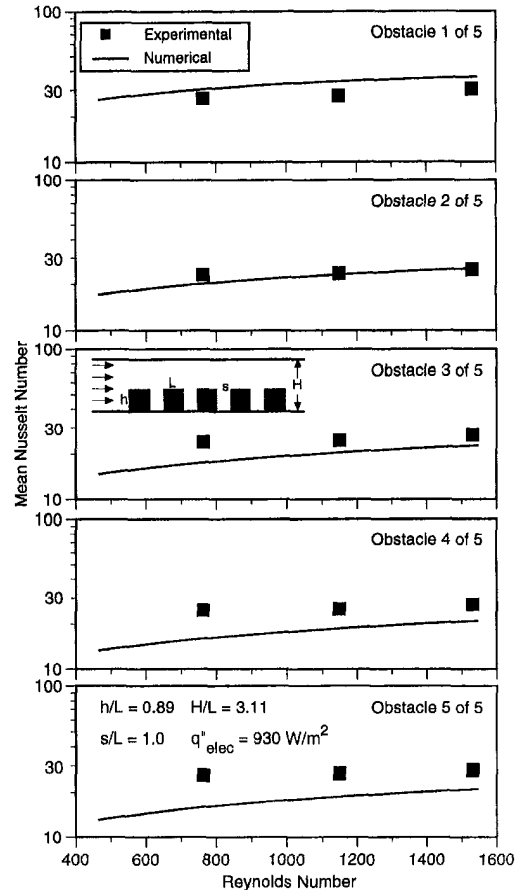


Fig. 7 Mean Nusselt number comparisons between the experimental and numerical results for a three obstacle array with  $h/L = 0.89$ ,  $s/L = 1.0$ ,  $H/L = 3.11$ , and  $q''_{elec} = 930 \text{ W/m}^2$

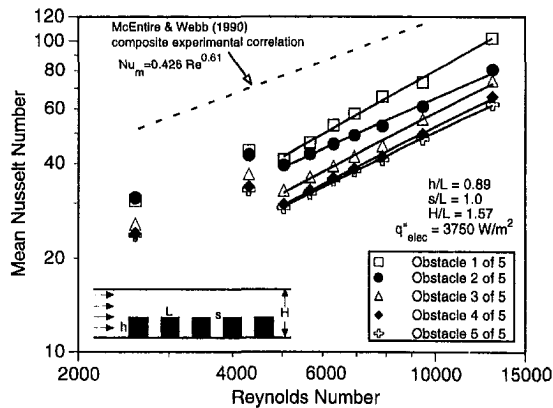


Fig. 8 Mean Nusselt numbers for the array of five identical obstacles with  $h/L = 0.89$ ,  $s/L = 1.0$ ,  $H/L = 1.57$ , and  $q''_{elec} = 3750 \text{ W/m}^2$

lation for the experimental data of Fig. 8, considering all five obstacles in the array

$$Nu_m = 0.186 Re_{D_h}^{0.61} \quad (14)$$

( $2500 \leq Re_{D_h} \leq 13000$ ), does exhibit nearly the same Reynolds number dependency.

The general trends in the obstacle mean Nusselt numbers are an increase with increased Reynolds numbers and a decrease with downstream obstacle position. At a Reynolds number of about 4500, however, the relationship between the Nusselt and Reynolds numbers changes. Dividing the data at this point and applying least-squares correlations using the equation

$$Nu_m = A Re_{D_h}^B \quad (15)$$

(with correlation coefficients greater than 0.99) shows a considerable difference in the Reynolds number exponents ( $B$ ), as shown in Table 1. This is perhaps attributable to the change in the flowfield from transitional to fully turbulent, though velocity surveys would be required to corroborate this point. The channel mean velocity at this flow rate is about 0.9 m/s. Arvizu and Moffat (1981) found that, in the fully developed regime of an array of obstacles,  $Nu_m \propto Re^{0.75}$ , which is similar to that reported here for downstream obstacles 2–5. The first obstacle in the array was found to have a greater Reynolds number exponent. This is due to the greater heat transfer along the upstream vertical face (**AB**) caused by core flow impingement. The downstream obstacles do not experience this heat transfer along their vertical faces because the core flow does not expand substantially into the interobstacle cavities and interact strongly with this fluid when the obstacles are moderately spaced ( $s/L = 1.0$ ).

Table 1 Mean Nusselt number correlation parameters for the five identical obstacle array with  $h/L = 0.89$ ,  $s/L = 1.0$ ,  $H/L = 1.57$ , and  $q''_{elec} = 3750 \text{ W/m}^2$

Obstacle Number	$Re_{D_h}$ Range	A	B
1	2600 - 4300	0.1262	0.699
	5000 - 13000	0.0140	0.940
2	2600 - 4300	0.2701	0.605
	5000 - 13000	0.0672	0.746
3	2600 - 4300	0.1028	0.703
	5000 - 13000	0.0212	0.860
4	2600 - 4300	0.1339	0.661
	5000 - 13000	0.0244	0.833
5	2600 - 4300	0.1661	0.632
	5000 - 13000	0.0338	0.794

$$Nu_m = A Re_{D_h}^B$$

$$h/L = 0.89, s/L = 1.0, H/L = 1.57, q''_{elec} = 3750 \text{ W/m}^2$$

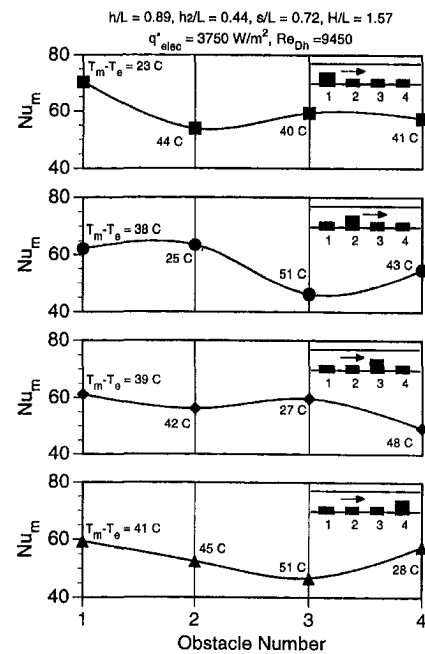


Fig. 9 Mean Nusselt numbers for the four obstacle array with one taller obstacle ( $h/L = 0.89$ ) systematically positioned in an array of obstacles with height  $h_2/L = 0.44$  ( $s/L = 0.72$ ,  $H/L = 1.57$ ,  $Re_{D_h} = 9450$ ,  $q''_{elec} = 3750 \text{ W/m}^2$ )

In order to quantify the effects caused by a taller obstacle upon the heat transfer from the remaining shorter obstacles in the array, in the thermal development region, experiments were performed for four ordered configurations. In these four cases the taller obstacle ( $h/L = 0.89$ ) was systematically located in the first through fourth positions in the array while the remaining three positions were populated with obstacles of height  $h_2/L = 0.44$ . All four of the obstacles were of the same length,  $L$ , the interobstacle spacing was maintained at  $s/L = 0.72$ , and the channel height was  $H/L = 1.57$ . The airflow rate was held at  $Re_{D_h} = 9450$  while the input electrical power to the heaters yielded  $q''_{elec} = 3750 \text{ W/m}^2$ .

When compared with the shorter obstacles in the array, the introduction of the taller obstacle into the array reduces the bypass area, causing the air flow rate to increase as it is diverted upwards away from the channel floor into the bypass region. Beyond the taller obstacle the core flow expands which, in the absence of further obstructions, would produce a large recirculation, with corresponding low fluid velocities, that would reattach to the channel floor downstream. The effect found here was, as expected, that the shorter obstacle immediately behind the taller obstacle always showed a decrease in mean Nusselt number, as shown in Fig. 9, and an increase in temperature difference ( $T_m - T_e$ ). It should be noted that the curves in Fig. 9 are for illustrative purposes to elucidate the trends in the mean Nusselt numbers for each of the obstacles in the arrays. The shorter obstacles further downstream, however, show an increase in Nusselt numbers. This increase is due to the reattachment of the expanding core flow, causing increased mixing and flow impingement upon these downstream obstacles.

The mean Nusselt numbers of the taller obstacle, at each position in the array, form an envelope under which the Nusselt numbers for the shorter obstacles remain below. The downstream obstacles with heat transfer enhancement due to flow impingement do, though, draw near to these values. The temperatures of the shorter obstacles, however, are always larger than that of the taller obstacle due to their reduced convective surface area. This result suggests that the proper placement of geometrically dissimilar obstacles, in this case a taller obstacle, can be

used to passively enhance the heat transfer for critical components in its vicinity, though, again, the temperature must be found to characterize the thermal state of the component. The proper tuning of such a system would be dependent upon the flow rate and geometries in order to control the reattachment zones and their subsequent convective augmentation. Since the current experimental configuration emphasizes the spanwise obstacle formation, the effect of the flow recirculation immediately behind the taller obstacle is further pronounced. Without streamwise flow passages between obstacles, there is no suction influence to draw the fluid in this low-velocity/high-pressure region away. The result is the heat transfer decrease immediately behind the taller obstacle.

## Conclusions

An experimental investigation was performed to determine the thermal effects of parametric changes to a modular airflow channel containing individual and arrays of heated two-dimensional obstacles. The effects of changes in the channel height, input heater power, and airflow rate upon the mean Nusselt numbers and surface temperature differences were documented for an individual as well as an array of obstacles within the channel. As expected, low flow rates were found to significantly increase the temperature of the obstacle due to reduced convective coefficients. Very large heater powers were also found to increase the obstacle temperature as the limits for sensible heat convective transport for air are approached. Large-obstacle temperature increases, the critical measure for electronic device failure, were explicitly detailed as they were found to be obscured by the Nusselt number due to its definition as a ratio. The experimental mean Nusselt numbers for individual and multiple obstacle arrays were found to be in good agreement with the numerical model. The mean heat transfer from individual and arrays of protruding heat sources within the channel was correlated with the airflow Reynolds number. For the individual obstacle, with  $h/L = 0.89$ ,  $H/L = 1.57$ , and  $q_{\text{elec}}'' = 8500 \text{ W/m}^2$ , the correlation obtained was

$$\text{Nu}_m = 0.4472 \text{Re}_{D_h}^{0.5618} \quad (800 \leq \text{Re}_{D_h} \leq 13000).$$

For the obstacle array with geometry  $h/L = 0.89$ ,  $s/L = 1.0$ ,  $H/L = 1.57$ , and  $q_{\text{elec}}'' = 3750 \text{ W/m}^2$ , correlations of the form  $\text{Nu}_m = A \text{Re}_{D_h}^B$  ( $2600 \leq \text{Re}_{D_h} \leq 13000$ ) were obtained for all five of the obstacles within the array, where  $A$  and  $B$  are given in Table 1. The position of a taller obstacle in an array was found to reduce the heat transport from the obstacle immediately behind it, though it also enhanced the thermal transport from obstacles further downstream that benefit from increased mixing and impingement as the core flow expands and reattaches. This passive heat transfer augmentation effect would require the synchronization of the airflow rate with the channel and obstacle geometries to control the reattachment region and its subsequent convective augmentation.

## Acknowledgments

The support of the Aerospace Power Division of the USAF Wright Laboratory under contract F3360196MT565 and Dr.

Jerry Beam, Deputy for Technology, is gratefully acknowledged.

One of the authors (KV) also wishes to acknowledge the support from CNR Bilateral Research project Grant No. 97.03198.CT07 while working on portions of this project.

## References

- Arvizu, D. E., and Moffat, R. J., 1981, "Experimental heat transfer from an array of heated cubical elements on an adiabatic channel wall," Report HMT-33, Thermosciences Division, Department of Mechanical Engineering, Stanford University, Stanford, CA.
- Cess, R. D., and Shaffer, E. C., 1959a, "Heat Transfer to Laminar Flow Between Parallel Plates with a Prescribed Wall Heat Flux," *Applied Scientific Research*, Vol. A8, pp. 339–344.
- Cess, R. D., and Shaffer, E. C., 1959b, "Summary of Laminar Heat Transfer Between Parallel Plates with Unsymmetrical Wall Temperatures," *J. Aero Space Sciences*, Vol. 26, p. 538.
- Davalath, J., and Bayazitoglu, Y., 1987, Forced Convection Cooling Across Rectangular Blocks, *ASME JOURNAL OF HEAT TRANSFER*, Vol. 109, pp. 321–328.
- FIDAP, 1993, *Theory Manual*, Fluid Dynamics International, Evanston, IL.
- Garimella, S. V., and Eibeck, P. A., 1990, Heat Transfer Characteristics of an Array of Protruding Elements in Single-Phase Forced Convection, *Int. J. Heat Mass Transfer*, Vol. 33, pp. 2659–2669.
- Jubran, B. A., Swiety, S. A., and Hamdan, M. A., 1996, "Convective heat transfer and pressure drop characteristics of various array configurations to simulate the cooling of electronic modules," *Int. J. Heat and Mass Transfer*, Vol. 39, pp. 3519–3529.
- Jubran, B. A., and Al-Salaymeh, A. S., 1996, "Heat transfer enhancement in electronic modules using ribs and 'film-cooling-like' techniques," *Int. J. of Heat and Fluid Flow*, Vol. 17, pp. 148–154.
- Kline, S. J., and McClintock, F. A., 1953, "Describing uncertainties in single-sample experiments," *Mechanical Engineering*, Jan., pp. 3–8.
- Lehmann, G. L., and Pembroke, J., 1991, Forced Convection Air Cooling of Simulated Low Profile Electronic Components: Part 1—Base Case, *ASME Journal of Electronic Packaging*, Vol. 113, pp. 21–26.
- Mahefkey, E. T., 1995, "High temperature (500–600 K) power electronics thermal management," *Proc. 12th Symposium on Space Nuclear Power and Propulsion*, American Institute of Physics, New York, pp. 917–929.
- McEntire, A. B., and Webb, B. W., 1990, "Local forced convective heat transfer from protruding and flush-mounted two-dimensional discrete heat sources," *Int. J. Heat and Mass Transfer*, Vol. 33, pp. 1521–1533.
- Moffat, R. J., 1988, "Describing the uncertainties in experimental results," *Experimental Thermal and Fluid Science*, Vol. 1, pp. 3–17.
- Molki, M., Faghri, M., and Ozbay, O., 1995, "A Correlation for Heat Transfer and Wake Effect in the Entrance Region of an In-Line Array of Rectangular Blocks Simulating Electronic Components," *ASME JOURNAL OF HEAT TRANSFER*, Vol. 117, pp. 40–46.
- Peterson, G. P., and Ortega, A., 1990, "Thermal control of electronic equipment and devices," *Advances in Heat Transfer*, Vol. 20, J. P. Hartnett and T. F. Irvine, eds., Academic Press, San Diego, pp. 181–314.
- Roeller, P. T., Stevens, J., and Webb, B. W., 1991, "Heat Transfer and Turbulent Flow Characteristics of Isolated Three-Dimensional Protrusions in Channels," *ASME JOURNAL OF HEAT TRANSFER*, Vol. 113, pp. 597–603.
- Sparrow, E. M., Yanezmoreno, A. A., and Otis, D. R., 1984, "Convective heat transfer response to height differences in an array of block-like electronic components," *Int. J. Heat and Mass Transfer*, Vol. 27, pp. 469–473.
- U. S. Department of Defense, 1991, "Reliability Prediction of Electronic Equipment," Military Handbook MIL-HDBK-217F, Washington, DC, Chapter 6.
- Vafai, K., and Kim, S. J., 1990, Analysis of Surface Enhancement by a Porous Substrate," *ASME JOURNAL OF HEAT TRANSFER*, Vol. 112, pp. 700–705.
- Young, T. J., and Vafai, K., 1998a, "Convective Cooling of a Heated Obstacle in a Channel," *Int. J. Heat Mass Transfer*, Vol. 41, pp. 3131–3148.
- Young, T. J., and Vafai, K., 1998b, "Convective flow and heat transfer in a channel containing multiple heated obstacles," *Int. J. Heat Mass Transfer*, Vol. 41, pp. 3279–3298.
- Zebib, A., and Wo, Y. K., 1989, A Two-Dimensional Conjugate Heat Transfer Model for Forced Air Cooling of an Electronic Device, *ASME Journal of Electronic Packaging*, Vol. 111, pp. 41–45.